

# Miniaturized laser heterodyne radiometer for measurements of CO<sub>2</sub> in the atmospheric column

E. L. Wilson · M. L. McLinden · J. H. Miller ·  
G. R. Allan · L. E. Ott · H. R. Melroy ·  
G. B. Clarke

Received: 21 November 2012 / Accepted: 25 May 2013 / Published online: 12 June 2013  
© The Author(s) 2013. This article is published with open access at Springerlink.com

**Abstract** We have developed a low-cost, miniaturized laser heterodyne radiometer for highly sensitive measurements of carbon dioxide (CO<sub>2</sub>) in the atmospheric column. In this passive design, sunlight that has undergone absorption by CO<sub>2</sub> in the atmosphere is collected and mixed with continuous wave laser light that is step-scanned across the absorption feature centered at 1,573.6 nm. The resulting radio frequency beat signal is collected as a function of laser wavelength, from which the total column mole fraction can be de-convolved. We are expanding this technique to include methane (CH<sub>4</sub>) and carbon monoxide (CO), and with minor modifications, this technique can be

expanded to include species such as water vapor (H<sub>2</sub>O) and nitrous oxide (N<sub>2</sub>O).

## 1 Introduction

Surface-observing networks have made major contributions to understand the carbon cycle as well as atmospheric distributions of key gases such as CO<sub>2</sub>, CH<sub>4</sub>, and CO. However, these observations have not been sufficient to constrain regional CO<sub>2</sub> fluxes, and many parameters related to the emission of these gases still vary widely. Significant uncertainty remains in the source and sink distributions of these gases as well as the processes that govern them and their interannual variability [1, 2]. Fluxes inferred from surface measurements alone are subject to errors in atmospheric transport models [3, 4]. However, vertical column measurements are less affected by model transport errors, making them particularly useful in constraining surface fluxes [5]. Rayner and O'Brien [6] demonstrated that monthly averaged column CO<sub>2</sub> from satellites with precisions of 2.5 ppmv on a 8 × 10° scale could provide a constraint on surface fluxes comparable to the existent surface network. A more recent study by Chevallier et al. [7] used data from 14 TCCON [8] stations to estimate fluxes and compared the results with estimates based on surface and aircraft observations. Their results indicated that TCCON-based flux estimates were consistent with northern hemisphere seasonal cycles and regional carbon budgets based on flux estimates using the in situ data sources. Though the TCCON results were less precise, in part due to the very sparse nature of the network, this demonstrated for the first time the utility of CO<sub>2</sub> column measurements in constraining carbon fluxes. The Chevallier et al. results

---

E. L. Wilson (✉) · G. R. Allan · H. R. Melroy · G. B. Clarke  
Laser Remote Sensing Laboratory, NASA Goddard Space Flight  
Center, 8800 Greenbelt Road, Greenbelt, MD 20771, USA  
e-mail: Emily.L.Wilson@nasa.gov

M. L. McLinden  
Microwave Instrument and Technology Branch, NASA Goddard  
Space Flight Center, 8800 Greenbelt Road, Greenbelt,  
MD 20771, USA

J. H. Miller · H. R. Melroy  
Department of Chemistry, George Washington University,  
725 21st Street, NW, Washington, DC 20052, USA

G. R. Allan  
Sigma Space Corporation, 4600 Forbes Blvd., Lanham,  
MD 20706, USA

L. E. Ott  
Global Modeling and Assimilation Office, NASA Goddard  
Space Flight Center, 8800 Greenbelt Road, Greenbelt,  
MD 20771, USA

G. B. Clarke  
American University, 4400 Massachusetts Avenue,  
Washington, DC 20016, USA

demonstrate the scientific value of a high-precision, ground-based, column observation network.

Here, we present a miniaturized laser heterodyne radiometer (mini-LHR) that measures CO<sub>2</sub> in the atmospheric column and offers a low-cost solution for filling in gaps in the current observational network. Miniaturization was possible through recent developments in the telecommunications industry that resulted in low-cost, commercially available, distributive feedback (DFB) lasers that produce stable near infrared light. The mini-LHR has been designed to operate in tandem with an AERONET sun tracker [9–11]. With more than 450 instrument sites worldwide, AERONET offers an established framework for future expansion of the mini-LHR and includes key arctic regions (not covered by GOSAT or the planned OCO-2 mission) [12] where release of CO<sub>2</sub> and CH<sub>4</sub> from thawing tundra and permafrost is a growing concern. An additional benefit to tandem operation with AERONET is the quantification of cloud and aerosol light scattering through simultaneous aerosol measurements. In their studies of sensitivity of a space-based measurement, Mao and Kawa [13] find that aerosol and cloud data are key to reduce errors in the CO<sub>2</sub> column because scattering by cloud and aerosol particles changes the pathlength of sunlight through the column and consequently changes the total column CO<sub>2</sub> absorption. A network of continuous, colocated measurements of CO<sub>2</sub> and aerosol abundance solves this pathlength issue and provides the opportunity to better understand the processes controlling carbon flux. Aerosols induce a radiative effect that is an important modulator of regional carbon cycles. Changes in the diffuse radiative flux fraction (DRF) due to aerosol loading have the potential to alter the terrestrial carbon exchange [6, 14].

## 2 Instrument design

### 2.1 Background of laser heterodyne radiometry

Since the 1970s, laser heterodyne radiometry has become a well established receiver technique [15–19] and has been used to measure atmospheric gases such as ozone (O<sub>3</sub>) [20, 21], water vapor (H<sub>2</sub>O) [22], methane (CH<sub>4</sub>) [22], ammonia (NH<sub>3</sub>) [23], and chlorine monoxide (ClO—an atmospheric free radical) [24], with efforts for additional species such as nitrous oxide (N<sub>2</sub>O) underway. We present a passive variation of the laser heterodyne radiometer that uses sunlight as the light source for absorption of CO<sub>2</sub> in the infrared. Sunlight is superimposed with laser light in a single mode fiber coupler. The signals are mixed in a fast photoreceiver, and the RF beat signal is extracted. Changes in concentration of the trace gas are realized through analyzing changes in

the beat frequency amplitude. Miniaturization is possible through the use of smaller DFB lasers and related fiber optic components that have recently become commercially available and inexpensive through progress in the telecommunications industry [9].

### 2.2 Atmospheric measurement approach

With the exception of satellite measurements such as GOSAT [25] and the upcoming OCO-2 mission [12, 26–28], there are two general approaches that are in regular use for measuring carbon cycle gases in the atmosphere: (1) in situ instruments that sample gases from a specific location and then analyze samples with an analytical instrument such as an infrared gas analyzer and (2) sun-tracking instruments that measure gases in the atmospheric column using sunlight as the light source for absorption measurements. FLUXNET [29] and NOAA's ESRL/GMD Surface flask sampling network [30] support the first type of measurement. These approaches offer global coverage, but because sampling occurs near the surface (and not in the entire atmospheric column), these measurements are typically not adequate for validation and calibration of satellite data. Other examples of the first type are NOAA's tall tower [31] and CCGG aircraft measurements [32]. These retrieve some altitude information—but are limited by the availability of tall tower sites and flight sampling locations. The second type of instrument measures gases in the atmospheric column and consequently provides a better comparison with satellite retrievals where trace gases are also measured in the column. The main network of these ground instruments, total carbon column-observing network (TCCON) [8], is comprised of 16 operational global instrument sites. TCCON data are already being used for validation of GOSAT [25] data and in the future, will be used for OCO-2 [33] validation. These Fourier-transform spectrometers (FTS) can measure the largest range of trace gases, but expansion of the network is limited due to cost.

The mini-LHR is in the second category of instruments and offers a low-cost solution for filling in gaps in the TCCON network with targeted measurements of key carbon cycle gases. The passive mini-LHR has been designed to operate in tandem with an AERONET sun photometer. With more than 450 instrument sites worldwide, AERONET offers an established framework for future expansion of the mini-LHR. While only CO<sub>2</sub> measurements are presented here, the mini-LHR can be expanded to include methane (CH<sub>4</sub>) and carbon monoxide (CO) measurements. Also, because the mini-LHR is operated in tandem with AERONET, it will be possible to identify interferences from cloud and aerosol scattering through simultaneous aerosol measurements.

### 2.3 Sun tracking and collimation

The mini-LHR uses the sun tracker technology of an AERONET sun photometer [9–11] for collection of sunlight in the atmospheric column. Collimation optics for the mini-LHR is noninvasively “piggy-backed” to the sun tracker through a custom-made lightweight band of aluminum (shown in Figs. 1, 3). While the mini-LHR collimation optics can be connected to a variety of different sun trackers, the AERONET sun tracker has been found to be reliable and the link to the AERONET network provides an existing global framework for future deployments of the mini-LHR. AERONET sun-tracking instruments are commercially produced by CIMEL Electronique (model CE 318, CIMEL.FR). A typical AERONET installation consists of three components: an optical head, an electronics box, and a robot. The optical head consists of two collimators (with and without lenses). The electronics box runs the motion control as well as the data collection through separate processors. The robot has two stepper motors that control the zenith and azimuth of the tracker which are

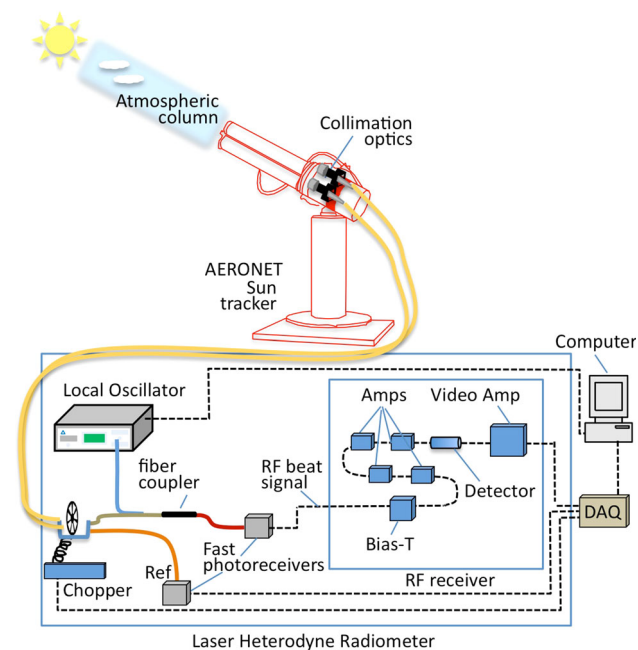


**Fig. 1** Schematic of the mini-LHR. Sunlight that has undergone absorption by CO<sub>2</sub> is collected with fiber-coupled collimation optics that is connected to an AERONET sun tracker. This incoming sunlight is chopped and then superimposed with light from the DFB laser (local oscillator) in a single mode fiber coupler. Superimposed light is mixed in an InGaAs detector (fast photoreceiver) to produce the RF beat signal. The RF receiver amplifies and detects the beat signal that is then measured through a data acquisition device that is synchronized with the chopper frequency. To measure the CO<sub>2</sub> absorption feature, the laser is scanned over the appropriate IR wavelength, and changes in the resulting RF beat signal are monitored

used in combination with a 4-quadrant detector for a tracking accuracy of better than 0.1°.

For AERONET data collection, these sun trackers operate every 15 min: returning to a “rest” position between measurements. For our experiments, we operated the sun tracker continuously with an update interval of 30 s. A single mode fiber optic cable brings light from the collimator into the mobile instrument. The field of view (FOV) for each of the collimators was  $\sim 0.2^\circ$  (compared to the  $1.2^\circ$  FOV of AERONET and the  $\sim 0.5^\circ$  FOV of the sun). The tracking accuracy of AERONET is 0.1° and results in a minor oscillation that can be seen in the baseline of the absorption scans. To mitigate this, a second LHR collimator serves as a reference channel to monitor the signal from the sun in this wavelength region. This channel is sensitive to the accuracy of the tracker as well as drops in the signal due to cloud cover or aerosols.

### 2.4 Miniaturized laser heterodyne radiometer (mini-LHR)

In this passive instrument, sunlight that has undergone absorption by CO<sub>2</sub> is collected and mixed with laser light that scans across a CO<sub>2</sub> absorption feature at 1,573.6 nm. This line was selected at a wavelength region that contains minimal interferences from other species such as water vapor, but also that was within the C–L bands for commercially available DFB lasers. A schematic of the instrument set-up is shown in Fig. 1. Incoming light is modulated with an optical chopper and introduced into the

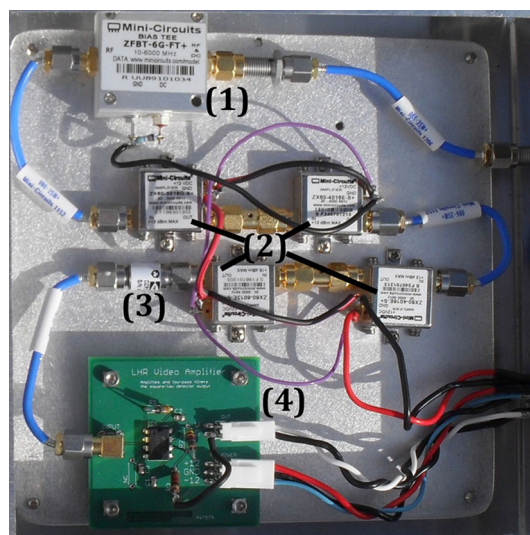


**Fig. 2** The compact RF receiver amplifies and detects the beat signal that is produced in the fast photoreceiver. Components from upper right include 1 bias tee with 50 ohm resistor, 2 high-gain, low-noise amplifiers, 3 square-law detector, and 4 video amplifier

mini-LHR through a single mode optical fiber. Light from the local oscillator (a DFB laser) is superimposed on this incoming sunlight in a 50/50 single mode fiber coupler. Superimposed light is mixed in a fast photoreceiver (a 5 GHz InGaAs detector) to produce an RF beat signal.

The beat signal enters the RF receiver/amplification stage (shown in Figs. 1, 2) through a bias tee with a 50 ohm resistor (the required InGaAs detector DC impedance) to separate RF and DC outputs of the InGaAs detector. The RF signal passes through a gain stage to amplify and set the bandwidth of the measurement (twice the RF bandwidth due to the double-sideband property of the optical-RF mixing). RF detection is performed with a square-law detector that outputs a voltage that is proportional to the square of the input voltage, allowing the measurement of the power of the RF signal. Output from the RF detector is amplified and low-pass filtered with a video amplifier circuit to produce a DC signal equal to the averaged power in the RF circuit over a chosen time interval. The final output voltage from the video amplifier is a chopped signal with the power of the input signal. When the optical chopper is blocking the incoming light, the RF subsystem output is proportional to the system noise. The amplitude of this chopped signal is monitored as the laser is scanned through the absorption feature and provides an output proportional to the incoming light around the laser wavelength with a bandwidth equal to twice the RF bandwidth. The instrument bandwidth/resolution was measured by mixing light from duplicate DFB lasers and measuring the emergence of the beat signal. The first laser was set to a constant wavelength and the second laser was scanned across the first wavelength while monitoring the beat signal after the RF subsystem. We found the bandwidth of the system to be  $\sim 1.3$  GHz ( $\sim 0.011$  nm at 1,573 nm).

## 2.5 Data acquisition

The small changes in the modulated signal amplitude due to perturbations in the CO<sub>2</sub> content within the planetary boundary layer are easily captured with a commercially available data acquisition cards, DAQ, of modest speed but high digitization fidelity. We use a National Instruments NI-USB-6255 16 bit digitizer operating at 20Ks/s to capture the variation in signal voltage from the two wide-band RF detection channels of the mini-LHR. The measured signals are a modulated, near square-wave voltage of a few 10–100 s of mV at 200 Hz with a 50/50 duty cycle. The DAQ is electronically triggered from the mechanical chopper, an SR540 chopper with negligible phase drift. The captured signals are process in real time using custom software written in LabVIEW running on a Windows laptop. The custom software essentially performs a boxcar operation to measure the amplitude of the modulation. The

amplitude of the signal and reference are then recorded as a function of wavelength for later analyses.

## 3 Experimental results

### 3.1 Measurements of CO<sub>2</sub> in the atmospheric column

The mini-LHR is being tested at NASA's Goddard Space Flight Center (38°59'33" N, 76°50'23" W). The LHR is located on the roof of a building, allowing for a clear view of the sky throughout the entirety of the day.

The LHR instrument is comprised of an AERONET sun tracker and a weatherproof module (shown in Fig. 3) that houses the laser, the chopper, the InGaAs detectors, and the electronic components of the instrument. The module was not originally thermally controlled with the exception of some ventilation. Because summer roof temperatures exceed the upper operating range of the laser and detectors (operating range for both is 0–40 °C), the module was moved to a climate-controlled shipping container that is held at 25 °C. Future versions of the module will include both thermal control and internal temperature monitoring to minimize temperature-related wavelength uncertainty.

Two collimators are attached by a mount fitted to the AERONET sun tracker (one for the collection of the heterodyne signal and other as a reference). The mounts have 4° of adjustment in both pitch and yaw axes. The collimators are aligned to collect the maximum amount of sunlight (generally 2–3 μW) in the morning, and they



**Fig. 3** The mini-LHR (shown housed in a weather-proof case) collects sunlight with fiber-coupled collimation optics connected to an AERONET sun tracker (shown at top of photo)

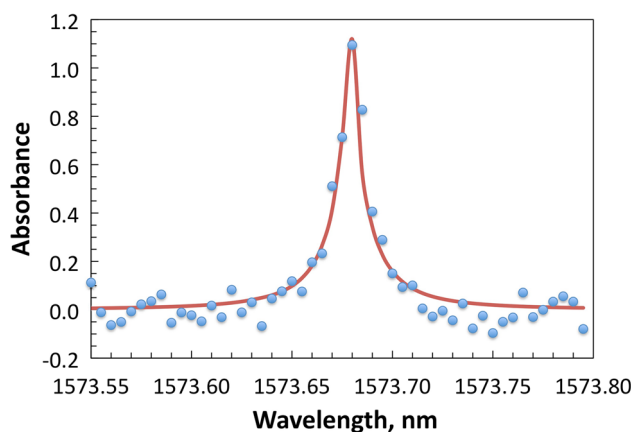


**Fig. 4** CO<sub>2</sub> measured in the atmospheric column. Data (shown as dots) has been fit with a simulated atmospheric absorption feature (line)

maintain good alignment throughout the day as the AER-ONET device tracks the sun. Sunlight is brought to the laser/detector module via FC/APC single mode fibers.

Figure 4 shows a typical measurement of CO<sub>2</sub> in the atmospheric column. The laser is scanned in 0.005 nm increments across the wavelength region of the absorption feature. Two-hundred data points are collected and averaged for an integration time of one second per increment. Raw data was fit with a simulated atmospheric CO<sub>2</sub> absorption feature, the details of which will be described in the following section.

### 3.2 Data handling and analysis

Raw data that have been collected from the LHR sensor are analyzed with a retrieval algorithm to (1) remove data outliers due to cloud and aerosol interferences, (2) remove data collected when the sun tracker was not able to lock onto the sun (due to weather or tracker maintenance issues), (3) fit the RF scans of the trace gas absorption features through a spectral simulation program (described below), and (4) extract mole fractions of the trace gases in the atmospheric column as a function of time of day.

For more than 20 years, a spectral simulation program, SpecSyn, has been under development at GWU [34–36]. For this project, SpecSyn is coupled with well known algorithms developed for atmospheric radiation transmission. For the latter, we borrow heavily from coding developed under the LOWTRAN and MODTRAN programs by AFOSR (and others) [37]. The interface between these two codes is detailed below.

In the case of light transmission through the atmosphere, it is necessary to account for variation of pressure, temperature, composition, and refractive index through the atmosphere that are all functions of latitude, longitude,

time of day, altitude, etc. The calculation of air mass is a well-studied problem, and sophisticated algorithms are available that can follow a light path through the atmosphere.

In MODTRAN (and most other air-mass calculations), the atmosphere is modeled as a series of spherically symmetric shells with boundaries specified at defined altitudes. Species mixing ratios are defined at the boundaries and are assumed to be invariant with each layer. Temperature and pressure are allowed to vary continuously with altitude as described below. In the case of the LHR instrument, the light path between an observer at the earth's surface and the sun passes through these layers and may be slightly curved due to variation in refractive index (See Fig. 5). The observed spectrum at the LHR instrument is the convolution of the contributions along this light path.

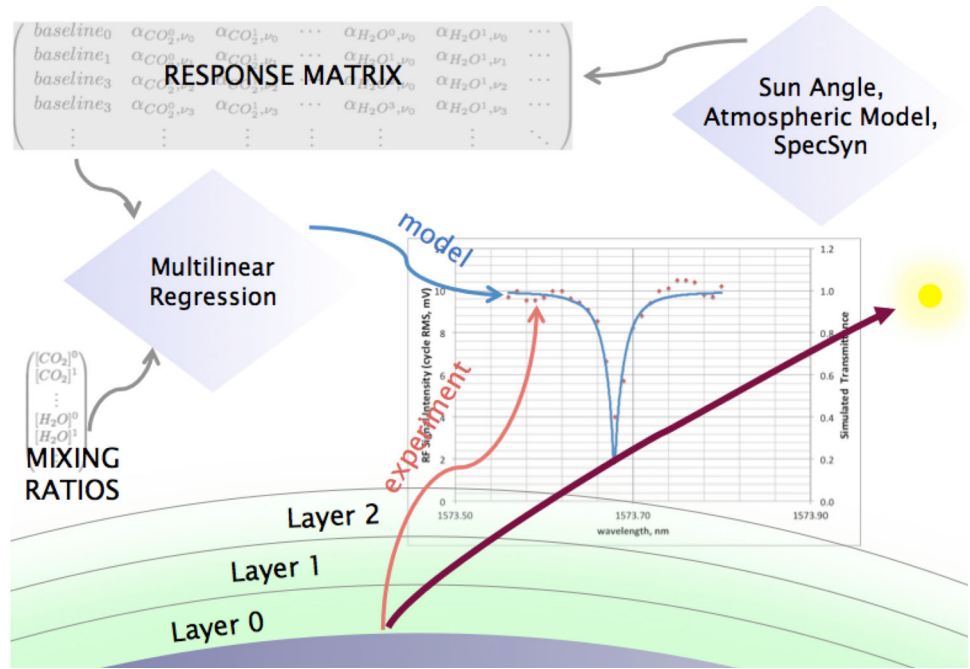
To quantify the composition for different layers, we implement a multilinear regression algorithm. For any absorption measurement the signal at a particular spectral frequency is a linear combination of spectral line contributions from several species. For each species that might absorb in a spectral region, we have precalculated its contribution as a function of temperature and pressure. The integrated path absorption spectrum can then be calculated using the initial sun angle (from location, date, and time) and assumptions about pressure and temperature profiles from an atmospheric model (as detailed in the MODTRAN documentation). Initial guesses for compositions of analytes and confounders at several atmospheric layer boundaries will be made from one of the six model atmospheres provided by MODTRAN. We will iterate the modeled spectrum to match the experimental observation using standard multilinear regression techniques. In addition to the layer concentrations, the numerical technique also provides uncertainty estimates for these quantities as well as dependencies on assumptions inherent in the atmospheric models.

For this initial proof-of-principle work, several simplifications are made in the light path definitions. First, refraction is ignored and the paths are assumed to be linear. This assumption is reasonable as most of the measurements reported here were made mid day (mostly in the 10:00 a.m.–2:00 p.m. window) in summer months, and thus with relatively small zenith angles (refraction is most important at larger zenith angles [37]).

For this work, estimates of the variation of temperature and pressure with altitude were extracted from the 1976 Standard US atmosphere (referenced as Model 6 in the Modtran2/3 Report [37]). The following empirical results were used in the data fits:

$$\ln(p(\text{torr})) = -1.49889 \times 10^{-1}Z(\text{km}) + 6.73791 \quad (1)$$

**Fig. 5** Illustration of data treatment algorithm. For each laser wavelength, a spectrum is collected at a sensor location and sun angle, time, and date are recorded. A standard atmospheric model is used as input to a SpecSyn calculation that calculates a response matrix with each species at each layer as the columns and spectral frequencies as the rows. Multilinear regression is then used to determine concentrations (e.g., [CO<sub>2</sub>] in layer 0, [CO<sub>2</sub>] in layer 1, etc.)



$$T(K) = 290.045 - 8.693378 Z(\text{km}) + 0.244606 [Z(\text{km})]^2 \tag{2}$$

For concentration determinations, 4 layers were considered in the atmosphere, defined at lower altitude boundaries of 0, 1, 5, and 10 km.

The resolution of the spectra collected using the mini-LHR is determined by the width of the RF filter spectral width, which here is less than line widths of the spectral features in the atmosphere. Thus, the variation of absorption with wavelength the Beer–Bouguer–Lambert Law gives the magnitude of the absorption:

$$\frac{I}{I_0} = \exp^{-S \times g(\nu) \times \rho \chi_j \times \ell} = \exp^{-\alpha \times \ell} \tag{3}$$

where  $S$  is the line strength of the absorption,  $g(\nu)$  is a line shape function,  $\rho$  is the gas density,  $\chi_j$  is the mole fraction of the absorber,  $\ell$  is the pathlength through the absorber, and  $\alpha$  is the extinction coefficient. In this case, transmitted near infrared light intensity is proportional to the measured RF power. The intensity of light in the absence of absorption can be determined by directly measuring solar intensity in a spectral absorption line, or by fitting a baseline from adjacent, nonabsorbing wavelengths. In either case, measured absorbance, defined in Eq. 3 is compared to that calculated using SpecSyn. Regression on the concentrations of analytes is then used to minimize differences between measured and modeled signals.

A Monte Carlo simulation was performed to assess sensitivity of reported concentrations to random noise in

absorbance data. The fitting program provides an option for fitting one or multiple concentrations of CO<sub>2</sub> in the atmospheric column. Not surprisingly, when multiple CO<sub>2</sub> concentrations were fit, a given noise in the spectrum produced a greater uncertainty in CO<sub>2</sub> concentrations than if a uniform atmospheric column concentrations is assumed.

### 3.3 Sensitivity estimate

Signal to noise ratio for the instrument was calculated from using the following equation,

$$S/N = 2\eta_e \sqrt{B\tau} T_0 / e^{\frac{h\nu}{\kappa T_{BB}}} - 1 \tag{4}$$

where  $T_{BB}$  is the temperature of the black body,  $\eta_e$  is the effective quantum efficiency of the InGaAs photodiode,  $B$  is the bandwidth of the intermediate frequency (or IF),  $\nu$  is the frequency,  $h$  is Planck’s constant,  $\kappa$  is Boltzmann’s constant,  $\tau$  is integration time and  $T_0$  is the total transmission factor [18]. Total transmission factor was estimated by combining expected optical loss. The optical loss in the system comes from coupling efficiency of the collimators, insertion loss of connecting fibers, chopping of the signal, phase misalignment, and polarization mismatch between the source and the local oscillator. Combining the sensitivity of the photodiode and the total transmission gave a total degeneracy factor of  $\sim 70 (1/\eta_e T_0)$ . For the instrument the SNR expanded with an increasing integration time according to Fig. 6.

For an integration time of one second, an estimated SNR of 477 was calculated. To measure the actual SNR, the data

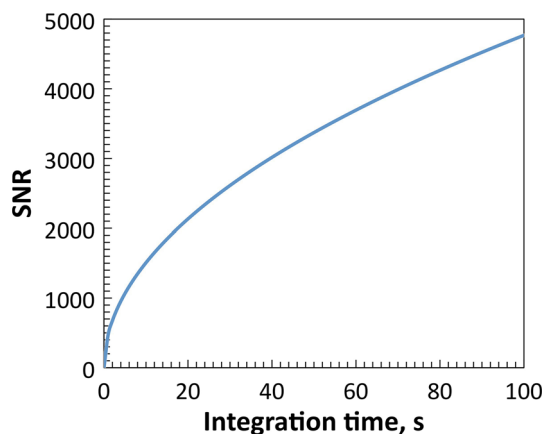


**Fig. 6** Calculated signal to noise ratio for the mini-LHR for integration times ranging from 0 to 100 s

from August 16, 2012 was utilized. This day was chosen because it was a particularly clear day in which consistently uninterrupted data was acquired. The baseline signal and uncertainty for each spectral sweep was calculated by fitting a Lorentzian line to the data. These values were then weighted together to give a final mean of baseline signal and uncertainty. The ratio of this output resulted in a measured SNR of 342. The difference in the calculated SNR and the measured SNR is most likely due to an under estimation of the effects of the beam filling factor, mixer-preamplifier noise, and lineshape distribution of signal.

Long-term stability of the components of the LHR instrument is a minor factor in the source of error. The local oscillator used in this setup is rated by the manufacturer at having a power stability of 0.01 dB, and a wavelength stability of 0.002 nm over a period of 24 h continuous use. The battery in the photodiode is rated for reliable operation for 190 mA h [38]. At the average power of the local oscillator this rating returns  $\sim 20$  h of reliable battery operation. This time is taken into account and batteries are frequently replaced for the photodiode.

The instrument sensitivity was estimated through Monte Carlo simulations that calculated the CO<sub>2</sub> concentration given varying levels of noise. Figure 7 shows the standard deviation in the calculated CO<sub>2</sub> as a function of absorbance noise. In this simulation, the concentration of CO<sub>2</sub> in the atmosphere was treated as a constant at 390 ppmv, and the zenith angle was assumed to be 25°. The noise intervals tested were 0.001, 0.002, 0.005, 0.01, 0.02, 0.05, and 0.1 which correspond to 0.1 % absorption, 0.2 % absorption, 0.5 % absorption, etc. The data was fitted with a power regression line. As shown in the fit, to achieve a sensitivity of 1 ppmv, noise in the measurement cannot exceed 1 %. Currently the measured instrument noise is approximately 10 % for 1 s of averaging of each data point corresponding to a sensitivity of  $\sim 8$  ppmv. Future improvements to the

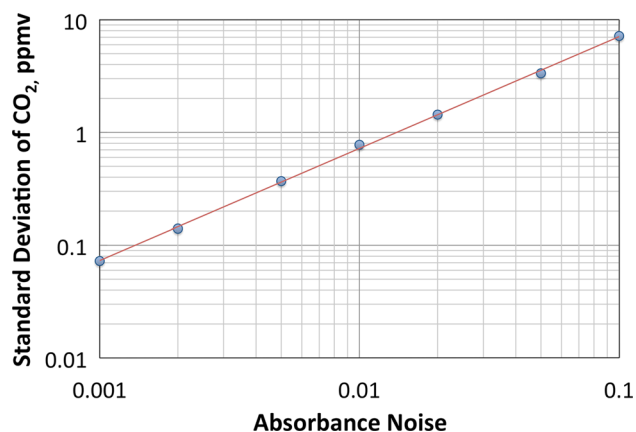


**Fig. 7** Simulations indicate that to achieve a 1 ppmv sensitivity, the noise in the measurement can not exceed 1 %

data acquisition speed and transitioning from laser step scanning to a modulated sweep scanning are anticipated to reduce this noise to the  $<1$  % requirement.

#### 4 Conclusions

We have presented a passive mini-LHR and preliminary measurements of carbon dioxide in the atmospheric column at 1,573.6 nm. The mini-LHR has been designed to operate in tandem with the passive aerosol sensor currently used in AERONET. Through leveraging of AERONET's existing global aerosol monitoring network, the mini-LHR has a clear pathway to future deployment in key locations that reduce flux uncertainty. Tandem operation will offer correction of cloud and aerosol light scattering through the simultaneous aerosol measurements. We report a precision of  $\sim 8$  ppmv for 1 s of averaging for column CO<sub>2</sub> measurements in cloud-free conditions with the current instrument configuration. Future changes in the data acquisition speed and laser scanning method are expected to improve this to a better than 1 ppmv.

**Acknowledgments** We would like to thank the NASA Goddard Space Flight Center's Internal Research and Development (IRAD) and Science Innovation Fund (SIF) programs for funding this effort. We would also like to thank Brent Holben and the entire AERONET team for their ongoing collaboration and support.

**Open Access** This article is distributed under the terms of the Creative Commons Attribution License which permits any use, distribution, and reproduction in any medium, provided the original author(s) and the source are credited.

#### References

1. IPCC, *Climate Change 2007: The Physical Science Basis. Contribution of Working Group I to the Fourth Assessment Report of*

- the Intergovernmental Panel on Climate Change* (Cambridge University Press, Cambridge, 2007)
2. B.C. Pak, M.J. Prather, CO<sub>2</sub> source inversions using satellite observations of the upper troposphere. *Geophys. Res. Lett.* **28**, 4571–4574 (2001)
  3. K.R. Gurney, R.M. Law, A.S. Denning, P.J. Rayner, B.C. Pak, T.L. Modelers, Transcom 3 inversion intercomparison: control results for the estimation of seasonal carbon sources and sinks. *Glob. Biogeochem. Cyc.* **18** (2004). doi:10.1029/2003GB002111
  4. D.F. Baker, et al., TransCom 3 inversion intercomparison: impact of transport model errors on the interannual variability of regional CO<sub>2</sub> fluxes, 1988–2003. *Glob. Biogeochem. Cyc.* **20**, doi:10.1029/2004GB002439 (2006)
  5. D. Wunch, G.C. Toon, J.F.L. Blavier, R.A. Washenfelder, J. Notholt, B. Connor, D.W.T. Griffith, V. Sherlock, P.O. Wennberg, The total carbon column observing network (TCCON). *Philos. Trans. R. Soc. Math. Phys. Eng. Sci.* **369**, 2087–2112 (2011)
  6. P.J. Rayner, D.M. O'Brien, The utility of remotely sensed CO<sub>2</sub> concentration data in surface source inversions. *Geophys. Res. Lett.* **28**, 175–178 (2001)
  7. F. Chevallier, et al., Global CO<sub>2</sub> fluxes inferred from surface air-sample measurements and from TCCON retrievals of the CO<sub>2</sub> total column. *Geophys. Res. Lett.* **38** (2011). doi:10.1029/2011GL049899
  8. *Total Carbon Column Observing Network (TCCON) of Ground-Based Fourier-Transform Spectrometers* (California Institute of Technology, Caltech, 2011), retrieved <https://tccon-wiki.caltech.edu>
  9. *AERONET Aerosol Robotic Network* (NASA Goddard Space Flight Center, 2011), retrieved <http://aeronet.gsfc.nasa.gov/>
  10. B.N. Holben, D. Tanre, T.F. Eck, I. Slutsker, N. Abuhassan, W.W. Newcomb, J. Schaefer, B. Chatenet, F. Lavenue, Y.J. Kaufman, J. Vande Castle, A. Setzer, B. Markham, D. Clark, R. Frouin, R. Halthore, A. Kamieli, N.T. O'Neill, C. Pietras, R.T. Pinker, K. Voss, G. Zibordi, An emerging ground-based aerosol climatology: aerosol optical depth from AERONET. *J. Geophys. Res.* **106**, 12067–12097 (2001)
  11. B.N. Holben, T.F. Eck, I. Slutsker, D. Tanre, J.P. Buis, A. Setzer, E. Vermote, J.A. Reagan, Y.J. Kaufman, T. Nakajima, F. Lavenue, I. Jankowiak, A. Smirnov, AERONET—a federated instrument network and data archive for aerosol characterization. *Remote Sens. Environ.* **66**, 1–16 (1998)
  12. *Orbiting Carbon Observatory-2* (NASA, 2012), retrieved <http://science.nasa.gov/missions/oco-2/>
  13. J.-P. Mao, S.R. Kawa, Sensitivity studies for space-based measurement of atmospheric total column carbon dioxide by reflected sunlight. *Appl. Opt.* **43**, 914–927 (2004)
  14. D. Niyogi, H.-I. Chang, V.K. Saxena, T. Holt, K. Alapaty, F. Booker, F. Chen, K.J. Davis, B.N. Holben, T. Matsui, T. Meyers, W.C. Oechel, R.A. Pielke, R. Wells, K. Wilson, Y. Xue, Direct observations of the effects of aerosol loading on net ecosystem CO<sub>2</sub> exchanges over different landscapes. *Geophys. Res. Lett.* **31**, L20506 (2004)
  15. R. T. Menzies, M. S. Shumate, in *Usefulness of the Infrared Heterodyne Radiometer in Remote Sensing of Atmospheric Pollutants*. Joint Conference on Sensing of Environmental Pollutants, pp. 1–4 (1971)
  16. D. Weidmann, D. Courtois, Infrared 7.6- $\mu\text{m}$  lead-salt diode laser heterodyne radiometry of water vapor in a CH<sub>4</sub>-air premixed flat flame. *Appl. Opt.* **42**, 1115–1121 (2003)
  17. T.A. Livengood, T. Kostiuik, G. Sonnabend, J.N. Annen, K.E. Fast, A. Tokunaga, K. Murakawa, T. Hewagama, F. Schmulling, R. Schieder, High-resolution infrared spectroscopy of ethane in Titan's stratosphere in the Huygens epoch. *J. Geophys. Res.* **111**, 1–10 (2006)
  18. R.T. Ku, D.L. Spears, High-sensitivity infrared heterodyne radiometer using a tunable-diode-laser local oscillator. *Opt. Lett.* **1**, 84–86 (1977)
  19. G. Sonnabend, D. Wirtz, R. Schieder, Evaluation of quantum-cascade lasers as local oscillators for infrared heterodyne spectroscopy. *Appl. Opt.* **44**, 7170–7172 (2005)
  20. D. Weidmann, W.J. Reburn, K.M. Smith, Retrieval of atmospheric ozone profiles from an infrared quantum cascade laser heterodyne radiometer: results and analysis. *Appl. Opt.* **46**, 7162–7171 (2007)
  21. A. Delahaigue, D. Courtois, C. Thiebaux, S. Kalite, B. Parvitte, Atmospheric laser heterodyne detection. *Infrared Phys. Technol.* **37**, 7–12 (1996)
  22. R.K. Seals Jr., Analysis of tunable laser heterodyne radiometry: remote sensing of atmospheric gases. *AIAA J.* **12**, 1118–1122 (1974)
  23. V. Zeninari, B. Parvitte, D. Courtois, A. Delahaigue, C. Thiebaux, An instrument for atmospheric detection of NH<sub>3</sub> by laser heterodyne radiometry. *J. Quant. Spectrosc. Radiat. Transf.* **59**, 353–359 (1998)
  24. R.T. Menzies, A re-evaluation of laser heterodyne radiometer CIO measurements. *Geophys. Res. Lett.* **10**, 729–732 (1983)
  25. *GOSAT Project: Greenhouse Gases Observing Satellite* (National Institute for Environmental Studies (NIES), 2011), retrieved 2011, <http://www.gosat.nies.go.jp/eng/gosat/page6.htm>
  26. in *The Orbiting Carbon Observatory (OCO) is a New Earth Orbiting Mission Sponsored by NASA's Earth System Science Pathfinder (ESSP) Program Scheduled for Launch in 2008*. The Jet Propulsion Laboratory leads the effort with Orbital Sciences Corporation and Hamilton Sundstrand Sensor Systems as Partners
  27. D. Crisp, R.M. Atlas, F.M. Breon, L.R. Brown, J.P. Burrows, P. Ciais, B.J. Connor, S.C. Doney, I.Y. Fung, D.J. Jacob, C.E. Miller, D.M. O'Brien, S. Pawson, J.T. Randerson, P.J. Rayner, R.J. Salawitch, S.P. Sander, B. Sen, G.L. Stephens, P.P. Tans, G.C. Toon, P.O. Wennberg, S.C. Wofsy, Y.L. Yung, Z. Kuang, B. Chudasama, G. Sprauge, B. Weiss, R. Pollock, D. Kenyon, S. Schroll, The orbiting carbon observatory (OCO) mission. *Adv. Space Res.* **34**, 700–709 (2004)
  28. R. Haring, R. Pollock, B. Sutun, D. Crisp, in *The Orbiting Carbon Observatory (OCO) Instrument Optical Design*. SPIE Curr. Dev. Lens Des. Opt. Eng. V, pp. 51–62 (2004)
  29. *FLUXNET: A Global Network, Integrating Worldwide CO<sub>2</sub> Flux Measurements* (Oak Ridge National Laboratory for the National Aeronautics and Space Administration, 2011), retrieved 2011, <http://www.fluxnet.ornl.gov/fluxnet/index.cfm>
  30. *Carbon Cycle Surface Flasks* (NOAA Earth System Research Laboratory, Global Monitoring Division) (2012), <http://www.esrl.noaa.gov/gmd/ccgg/tables/>
  31. *NOAA ESRL GMD Tall Tower Network* (National Oceanic & Atmospheric Administration (NOAA): Earth System Research Laboratory (ESRL)/Global Monitoring Division (GMD), 2011), retrieved <http://www.esrl.noaa.gov/gmd/ccgg/towers/index.html>
  32. *Carbon Cycle Greenhouse Gases (CCGG) Aircraft Program* (National Oceanic and Atmospheric Administration (NOAA): Earth System Research Laboratory (ESRL)/Global Monitoring Division (GMD), 2011), retrieved <http://www.esrl.noaa.gov/gmd/ccgg/aircraft/>
  33. *Orbiting Carbon Observatory (OCO)* (Jet Propulsion Laboratory (JPL), California Institute of Technology, 2011), retrieved <http://oco.jpl.nasa.gov/observatory/>
  34. J.H. Miller, S. Elreedy, B. Ahvazi, F. Woldu, P. Hassanzadeh, Tunable diode-laser measurement of carbon monoxide concentration and temperature in a laminar methane-air diffusion flame. *Appl. Opt.* **32**, 6082–6089 (1993)
  35. M.P. Tolocka, J.H. Miller, Detection of polyatomic species in non-premixed flames using tunable diode laser absorption spectroscopy. *Microchem. J.* **50**, 397–412 (1994)



36. J.H. Miller, A.R. Awtry, M.E. Moses, A.D. Jewell, E.L. Wilson, in *Measurements of Hydrogen Cyanide and its Chemical Production Rate in a Laminar Methane/Air, Non-premixed Flame Using cw Cavity Ringdown Spectroscopy*. 29th Symposium (International) on Combustion (The Combustion Institute, 2002)
37. F.X. Kneizys, L.W. Abreu, G.P. Anderson, J.H. Chetwynd, E.P. Shettle, A. Berk, L.S. Bernstein, D.C. Robertson, P. Acharya, L.S. Rothman, J.E.A. Selby, W.O. Gallery, S.A. Clough, *The MODTRAN 2/3 Report and LOWTRAN 7 MODEL* (1996)
38. *Technical Data for SIR5-FC* (Thorlabs, Newton, 2012), retrieved [https://www.thorlabs.com/NewGroupPage9.cfm?ObjectGroup\\_ID=1297&pn=SIR5-FC#6297](https://www.thorlabs.com/NewGroupPage9.cfm?ObjectGroup_ID=1297&pn=SIR5-FC#6297)